Journal of Sol-Gel Science and Technology (2022) 101:420–427
https://doi.org/10.1007/s10971-021-05702-y

ORIGINAL PAPER: SOL-GEL AND HYBRID MATERIALS FOR DIELECTRIC, ELECTRONIC, MAGNETIC AND FERROELECTRIC APPLICATIONS

Mechanism of improving ferroelectric properties of $BiFe_{0.98}M_{0.02}O_3$ (M = Zn, Al, Ti) polycrystalline films

Guo-Dong Zhang[1] · Jian-Qing Dai[1] · Chang-Chang Zhang[1] · Xia-Li Liang[1]

Received: 18 July 2021 / Accepted: 3 December 2021 / Published online: 17 January 2022

Abstract

Pure $BiFeO_3$ (BFO) and (Zn^{2+}, Al^{3+}, Ti^{4+}) mono-doped $BiFe_{0.98}M_{0.02}O_3$ (M = Zn, Al, Ti) polycrystalline multiferroic films has been successfully synthesized on FTO/glass substrates via sol–gel spin-coating method. Effects of mono-doping with three different valence metal ions (Zn^{2+}, Al^{3+}, Ti^{4+}) on crystalline structure, surface morphology, and electrical properties of BFO films were systematically investigated. X-ray diffraction (XRD) results show that BFO film samples mono-doped with Zn^{2+}, Al^{3+}, and Ti^{4+} all have rhombic distorted perovskite structure of R3m space group, and no heterophases are produced. Scanning electron microscope (SEM) images reveal that microstructural density of $BiFe_{0.98}M_{0.02}O_3$ (M = Zn, Al, Ti) films is significantly increased compared to pure BFO. Furthermore leakage current densities of $BiFe_{0.98}M_{0.02}O_3$ (M = Zn, Al, Ti) films all reach up to the order of 10^{-5} A/cm^2 under applied electric field of 150 kV/cm, that is about three orders of magnitude lower than pure BFO films. Greatly reduced leakage current density confers superior ferroelectric properties to $BiFe_{0.98}M_{0.02}O_3$ (M = Zn, Al, Ti) films, as evidenced by beautiful *P*–*E* hysteresis loops at room temperature for (Zn^{2+}, Al^{3+}, Ti^{4+}) mono-doped $BiFe_{0.98}M_{0.02}O_3$ (M = Zn, Al, Ti) films and significantly higher double remnant polarization ($2P_r$ ~ 164.75–168.66 μC/cm^2) values compared to pure BFO (102.36 μC/cm^2). The significantly improved ferroelectric properties provide a new reference for the practical application of BFO film.

Graphical Abstract

The BFO, BFZO, BFAO, and BFTO films: (a) Polarization–electric field hysteresis loops diagram (*P*–*E*); (b) Leakage current–electric field diagram (*L*–*E*).

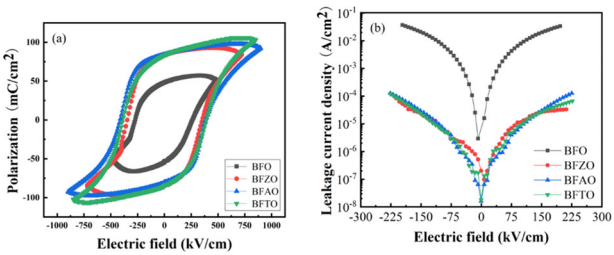

Keywords Sol–gel preparation · Thin films · (Zn^{2+}, Al^{3+}, Ti^{4+}) doping · $BiFe_{0.98}M_{0.02}O_3$ (M = Zn, Al, Ti) films · Ferroelectric property

1 Introduction

As a typical single-phase multiferroic material, $BiFeO_3$ (BFO) shows both ferroelectricity and G-antiferromagnetism at room temperature for the high Curie temperature (T_C ~ 1103 K) and the high Neel temperature (T_N ~ 643 K), as well as low crystallization

✉ Jian-Qing Dai
djqkust@sina.com

[1] Faculty of Materials Science and Engineering, Kunming University of Science and Technology, Kunming 650093, PR China

temperature and excellent theoretical remnant polarization (90–150 μC/cm^2) [1–4]. Compared with the traditional lead-based ferroelectric material, lead zirconate titanate (PZT), BFO is more environmentally friendly and also has superior theoretical performance. Therefore, BFO has become the most popular material in the research field of multiferroic materials. It is expected to replace the widely used commercial PZT and be applied for preparation of new practical information storage devices [5].

At present, the preparation process of BFO film is still not satisfactory as the prepared BFO film suffers from serious leakage current problem, which is also the major obstacle in the practical application of BFO in ferroelectric storage devices [5–7]. The leakage current mainly comes from the generation of heterophases, Bi vacancies, and oxygen vacancies [8, 9]. Heterogeneous phases are typically generated from impurities of Bi-rich phase $Bi_{25}FeO_{39}$ and Fe-rich phase $Bi_2Fe_4O_9$ caused by the high-temperature decomposition of BFO or the imbalance of stoichiometric ratio [10, 11]. By optimizing the process parameters during the preparation of films, the leakage current caused by the impurity phase can be prevented [12, 13]. Bi vacancies are mainly formed by the volatilization of Bi element during high-temperature annealing, which leads to stoichiometric mismatch and increase in leakage current. Generally, the problem of Bi vacancies can be effectively solved by using excess content of Bi in the batching process [14, 15].

Element doping, as one of the most effective methods, can effectively overcome the leakage current problem. In general, transition metal ions such as Cr^{3+}, Mn^{4+}, Ni^{2+}, Al^{3+}, and Ti^{4+}, which have similar radius and electronegativity as Fe^{3+}, can be used for doping Fe sites. These ions can accurately occupy the Fe site and effectively inhibit the fluctuation of Fe valence. Based on the theory of defect chemistry, heterovalent ion doping at Fe site can affect the valence state of Fe element and the concentration of oxygen vacancies can be altered due to charge compensation [16]. Yang et al. systematically studied the influence of mono-doping of +2 metal ions (Cu^{2+}, Zn^{2+}, Mn^{2+}) at Fe site on the leakage current of spin-coated films [17]. They concluded that the low-valence ions substituted at Fe site can combine with oxygen vacancies to produce $\left[\left(L_{Fe^{3+}}^{2+}\right)' - (V_{O^{2-}})^{\cdot\cdot}\right]$ defect complexes, which can limit the movement of $(V_{O^{2-}})^{\cdot\cdot}$ and thus making the leakage current lower. However, the ferroelectric hysteresis loops of the tested films were not well-saturated. Liu et al. found that high-valence Ti^{4+} doping at Fe site greatly reduced the leakage current density of films. They suggested that the charge compensation effect of Ti^{4+} limited the $Fe^{3+}\rightarrow Fe^{2+}$ transition *n*, thus making the oxygen vacancy concentration down meanwhile lowering the leakage current. However, the ferroelectric properties of their BFTO films were poor (2 $P_r \sim 3.8$ μC/cm^2) [18].In the exising research, Zhang et al. had been reported about Al^{3+} doping can lessen the leakage current of BFO films by three orders of magnitude, which was attributed to the lessened grain size and lower oxygen vacancy concentration due to Al^{3+} doping. However, why the ferroelectric properties exhibited improved by the undoped BFO films in their work is still not known [19].

Based on the above analysis, in this paper, $BiFe_{0.98}M_{0.02}O_3$ (M = Zn, Al, Ti) spin- coated films mono-doped with three different valence metal ions (Zn^{2+}, Al^{3+}, Ti^{4+}) at Fe site were fabricated (abbreviated as BFZO, BFAO, and BFTO, respectively). The structure, morphology, and electrical properties of the mono-doped BFZO, BFAO, and BFTO spin-coated films were systematically investigated. At the same time, the effect of doping different chemical valences at the Fe site on the BFO film is studied, which has not been done in the previous work.

2 Experimental

2.1 Synthesis

Zn^{2+}, Al^{3+}, and Ti^{4+} mono-doped $BiFe_{0.98}M_{0.02}O_3$ (M = Zn, Al, Ti) and pure BFO spin-coated films were prepared on FTO/glass substrate by sol–gel method. First, bismuth nitrate, iron nitrate, and nitrides of doping ions were weighed according to a certain stoichiometric ratio and added to a solvent mixture of ethylene glycol methyl ether and acetic acid with an accurate volume of 1:3. The mixture was stirred magnetically at room temperature until completely homogeneous. Then, a certain proportion of citric acid was added as a chelating agent (the stoichiometric ratio of citric acid to cations is 1.15:1), an appropriate amount of ethylene glycol was added to make the raw materials disperse evenly (the volume ratio of ethylene glycol and acetic is 1:8), and a suitable amount of ethanolamine was added to stabilize the dispersion (the volume ratio of ethanolamine and ethylene glycol is 1:1). Next, stirring was continued until a clear reddish-brown precursor solution was obtained, and the volume was adjusted to finally obtained a precursor solution with a concentration of 0.25 M. Finally, the precursor solution aged for 48 h was spin-coated onto FTO/glass substrate at 4000 rpm for 15 s. The deposited film was dried at 85 °C for 10 min and annealed at 550 °C for 10 min. Using layer-by-layer annealing, the above process was repeated 14 times to produce a spin-coated film with the required thickness.

2.2 Characterization

Using an X-ray diffractometer (XRD, Ultima IV, Japan) and a Raman spectroscope (LabRAM HR Evolution, France) to

analyze the crystal phases and structures of the spin-coated films. Microscopic morphology of the films was observed by a scanning electron microscope (SEM, S4800, Japan). To obtain the chemical valence states of the films, an X-ray photoelectric spectroscopy (XPS, ESCALAB 259xi, America) was used for charaterization. A ferroelectric analyzer (TF Analyzer 2000, aixACT company, Germany) was used for measuring ferroelectric loops and leakage current. A precision impedance analyzer (42954A, Agilent, USA) was used to measure dielectric constant and dielectric loss in the frequency range of 40 Hz–110 MHz with impedance accuracy of ±0.08%.

3 Results and discussion

3.1 structure and morphology

XRD patterns of BFO, BFZO, BFAO, and BFTO films are presented in Fig. 1, which Cu target Kα ray wavelength is 0.1504 nm is used as the light source, the scanning angle is 20–60°, and the width is 0.02°. As can be seen in Fig. 1a, no peaks for heterogeneous phases appear in these film samples, except for the FTO substrate diffraction peaks, indicating that the films are pure phases without the formation of secondary phases. The main diffraction peaks of the films can find to perfectly match with the standard PDF card (No: 73-0548). The films have a randomly oriented polycrystalline structure which belong to distorted rhombic perovskite structure with R3m space group. The main crystal phases of all the films are (100), (110) and (1$\bar{1}$0) orientations, and the strongest peaks are double peaks composed of (110) and (1$\bar{1}$0). This indicates that (Zn^{2+}, Al^{3+}, Ti^{4+}) mono-doping does not change the growth mode of the films. In addition, the (1$\bar{1}$0) diffraction peak intensity of BFZO and BFAO films increases significantly, while that of BFTO films decreases significantly, which indicates that Zn^{2+} and Al^{3+} doping improves the crystallinity of BFO films, while Ti^{4+} doping lowers the crystallinity of BFO. This effect may be

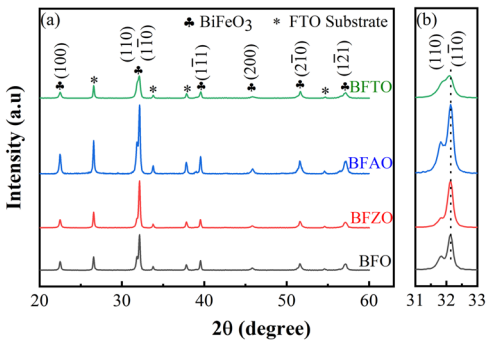

Fig. 1 XRD patterns of pure BFO and $BiFe_{0.98}M_{0.02}O_3$ (M = Zn, Al, Ti) films, **a** 2θ in the range of 20–60°. **b** 31–33° local magnification

attributed to the deformation of the crystal structure of BFTO film caused by Ti^{4+} doping, which is consistent with investigations described by Sharman [20]. The tendency of the (110) and (1$\bar{1}$0) double peaks of BFTO films to merge into a single peak is evident in Fig. 1b, which further confirms that Ti^{4+} doping causes greater deformation of the lattice structure.

Figure 2 shows the surface micro-morphology of BFO, BFZO, BFAO, and BFTO films, and the insets appear the corresponding cross-sectional morphology. It can be observed that there are many pinhole defects on the surface of pure BFO film, which drastically reduce the density of the film. However, the densities of BFZO, BFAO, and BFTO films increase markedly, which indicates that (Zn^{2+}, Al^{3+}, Ti^{4+}) mono-doping can improve the density of films, and improve their surface morphology. This will help to block the current leakage channel of the films, thus helping to improve the electrical properties of the films. From the cross-sectional view, it can be seen that pure BFO film has a blurred interface with FTO, while BFZO, BFAO, and BFTO films have a clear contact interface with the substrate, indicating that no mutual diffusion occurs. The cross-sectional thicknesses of BFO, BFZO, BFAO, and BFTO are 1040, 852, 889, and 864 nm, respectively, indicating that (Zn^{2+}, Al^{3+}, Ti^{4+}) mono-doping can lessen the thickness of the films and improve the bonding of the films to the interface.

3.2 Raman and XPS

In addition, the evolution of the film structure was analyzed by Raman spectroscopy. To obtain accurate peak positions of the vibrational modes, the Raman spectra of pure $BiFeO_3$ and $BiFe_{0.98}M_{0.02}O_3$ (M = Zn, Al, Ti) films were fitted by Gaussian fitting. As stated by the factor group theory, there are eight phonon modes in the BFO films, which is consistent with the literature on rhombic structured BFO films [21]. The A-mode at low frequencies corresponds to Bi-O bond vibration in BFO, while the E-mode at high frequencies is connected to Fe–O bond vibration [22]. Raman spectra of pure BFO and $BiFe_{0.98}M_{0.02}O_3$ (M = Zn, Al, Ti) films are shown in Fig. 2. A_1 modes of BFZO and BFTO films are significantly shifted toward lower frequencies compared to pure BFO, due to the distortion of the lattice structure due to doping. On the other hand, E-8 and E-9 modes exhibit some degree of broadening, which is mainly due to the distorted deformation of the $(Fe/Zn/Ti)O_6$ octahedral [23]. Furthermore, Raman spectra of BFAO films do not show any significant change compared with pure BFO, indicating that Al doping has a small effect for the structure of BFO films (Fig. 3).

In order to characterize the chemical bonding in the films, the survey spectra of the elements in the films and the

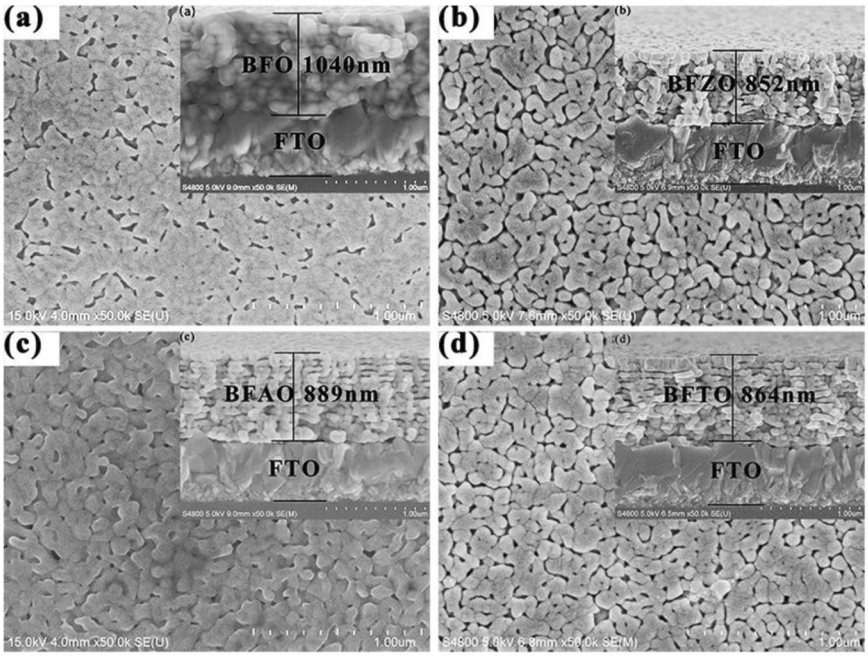

Fig. 2 Surface morphology of pure BFO and $BiFe_{0.98}M_{0.02}O_3$ (M = Zn, Al, Ti) films, where the insets show the respective cross-sectional morphology

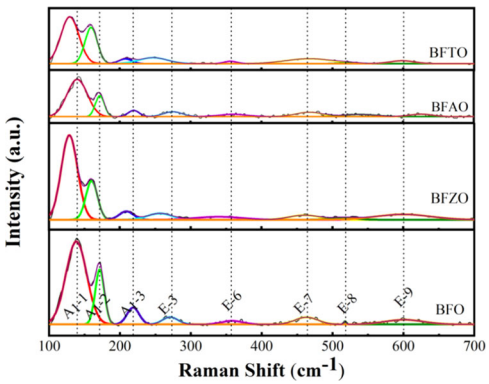

Fig. 3 Raman spectra of pure BFO and $BiFe_{0.98}M_{0.02}O_3$ (M = Zn, Al, Ti) films

valence bands of core levels were studied through XPS. The XPS survey spectra are extended from 0 to 1300 eV in the Fig. 4a. The mono-doped $BiFe_{0.98}M_{0.02}O_3$ (M = Zn, Al, Ti) films show no significant difference compared to the pure BFO owing to the small amount of doping. Figure 4b shows the XPS spectra of Fe from 700 to 740 eV. The Fe $2p_{3/2}$ and Fe $2p_{1/2}$ spin-orbit doublet components of the Fe 2p photoelectrons are located at around 710.4 and 724.5 eV, respectively. The above results confirm the coexistence of Fe^{2+} and Fe^{3+} in the film [24]. In the above peaks, the lower one (O_L) is the O^{2-} ions peak on the lattice sites of BFO, while the higher peak (O_H) is connected to the anoxic regions. This will also lead to decrease in oxygen vacancy concentration, because oxygen vacancies can serve as a bridge between Fe^{3+} and Fe^{2+} in the lattice. It has been reported that more Fe^{2+} ions signify more oxygen vacancies and lagrer leakage current density [25].

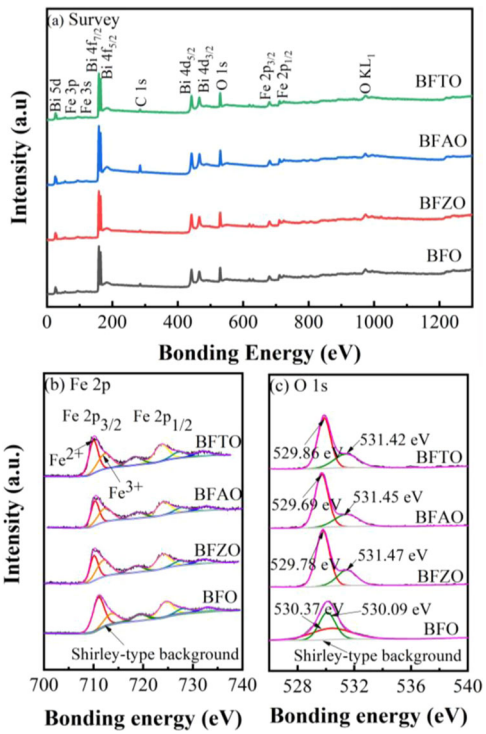

Fig. 4 **a** XPS survey spectra, **b** Fe 2p, **c** O 1s core levels of pure BFO and $BiFe_{0.98}M_{0.02}O_3$ (M = Zn, Al, Ti) films

To explore the effects of mono-doping with Zn^{2+}, Al^{3+}, and Ti^{4+} at Fe site on the oxygen state, the O 1s peaks in all films were measured and the results were summarized in Fig. 4c. There are two peaks at 530.09/530.37, 529.78/531.47, 529.69/531.45, and 529.86/531.42 for the four samples correspond to two kinds of oxygen atoms. In the

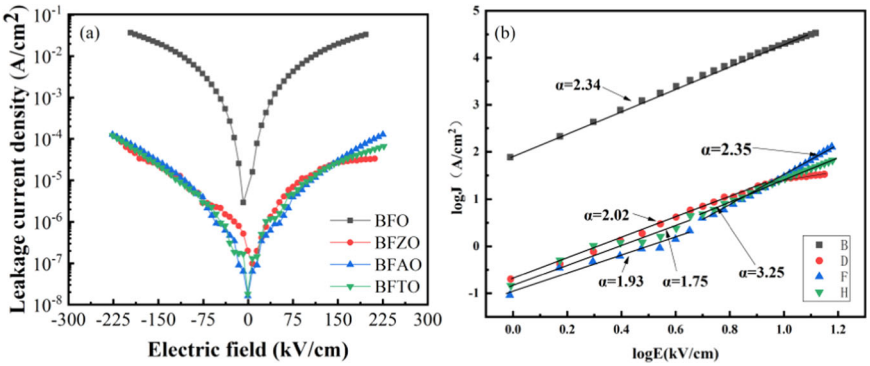

Fig. 5 **a** Leakage current-electric field diagram (*L-E*) for pure BFO and $BiFe_{0.98}M_{0.02}O_3$ (M = Zn, Al, Ti) films and **b** the Log (*J*) – Log (*E*) characteristics of BFO and $BiFe_{0.98}M_{0.02}O_3$ (M = Zn, Al, Ti) films

above peaks, the lower one (O_L) is the O^{2-} ions peak on the lattice sites of BFO, while the higher peak (O_H) is connected to the anoxic regions. By integrating the above two peaks to calculate their intensities, the oxygen vacancy contents in pure BFO, BFZO, BFAO and BFTO films are found to be 50, 28, 29 and 33% respectively. Therefore, (Zn^{2+}, Al^{3+}, Ti^{4+}) mono-doping significantly reduces the content of oxygen vacancies in BFO films.

3.3 Leakage current and *P–E* loops

The curves of leakage current density versus electric field (*L–E*) for BFO, BFZO, BFAO, and BFTO films are shown in Fig. 5. It can be seen that (Zn^{2+}, Al^{3+}, Ti^{4+}) mono-doped BFO films have significantly lower leakage current density. Furthermore, the leakage current magnitudes of BFZO, BFAO, and BFTO films are relatively close and have approximately the same trend as the electric field variation. The leakage current density values corresponding to BFO, BFZO, BFAO, and BFTO films are 2.03×10^{-2}, 2.73×10^{-5}, 2.98×10^{-5}, and 2.75×10^{-5} A/cm^2, respectively. The leakage currents of (Zn^{2+}, Al^{3+}, Ti^{4+}) mono-doped BFO films are all about three orders of magnitude lower compared to the pure BFO films. The reasons for this phenomenon can be explained as follows: (1) Zn^{2+} doping introduces $\left(Zn_{Fe^{3+}}^{2+}\right)'$, which can inhibit the valence fluctuation of Fe^{3+} to Fe^{2+}, reduce the concentration of $(V_{O^{2-}})^{\cdot\cdot}$, and also combine with $(V_{O^{2-}})^{\cdot\cdot}$ to form $\left[\left(Zn_{Fe^{3+}}^{2+}\right)' - (V_{O^{2-}})^{\cdot\cdot}\right]$ defect complexes, which has a positive effect on restricting the free movement of oxygen vacancies. (2) The partial replacement of Fe sites by Al^{3+} reduces the valence fluctuation of Fe^{3+}, which in turn reduces the concentration of oxygen vacancies. In general, the moving oxygen vacancy is the donor capture center of the electron, and the energy level of the oxygen vacancy is very close to the conduction band. Hence, the electron can be excited and conducted [26]. Consequently, the reduced concentration of oxygen vacancies by Al^{3+} doping will lead to the reduction of the leakage current density. (3) It has been reported that the doping of Fe sites by high-valence transition metal ions can effectively neutralize the charge defects by charge compensation effect [27, 28]. Therefore, partial replacement of Fe^{3+} sites by Ti^{4+} can inhibit the reduction of Fe^{3+}, which results in a lower concentration of oxygen vacancies and reduces the leakage current of films. (4) The SEM results show that (Zn^{2+}, Al^{3+}, Ti^{4+}) mono-doping can improve the density of the film. Higher density can reduce the transport channel of defect carriers, leading to leakage current of films decreasing.

To further investigate the influence of Zn, Al, Ti doping on the leakage mechanism of the BFO films, the log *J*–log *E* curves of BFMO (M = Zn, Al, Ti) films under positive electric field are presented in Fig. 5b. Based on the power law $J \propto E^{\alpha}$ relationship, the leakage current curves for the BFO and $BiFe_{0.96}M_{0.02}O_3$ films can be divided into several sections by piecewise linear fitting and the slope value of each segment is calculated from the fitting. Information on the conduction mechanism of each part can be inferred from the slope value α. It can be seen from the fitted slope values that all belong to the space-charge-limited current mechanism ($\alpha \sim 2$).

Figure 6 shows the polarization–electric field (*P–E*) hysteresis loops of pure BFO, BFZO, BFAO, and BFTO films at room temperature. The pure BFO has low anti-breakdown voltage and the *P–E* loop is extremely unsaturated. In contrast, BFO films mono-doped with (Zn^{2+}, Al^{3+}, Ti^{4+}) not only have more saturated *P–E* hysteresis loops but also significantly higher remnant polarization values. The $2P_r$ and $2E_c$ values measured at 1000 Hz for BFO, BFZO, BFAO, and BFTO films are 102.36 μC/cm^2 (535.86 kV/cm), 164.75 μC/cm^2 (704.50 kV/cm), 168.66 μC/cm^2, (798.86 kV/cm) and 168.24 μC/cm^2 (784.00 kV/cm), respectively. The improved ferroelectric properties of BFZO film may be mainly attributed to the introduction of $\left(Zn_{Fe^{3+}}^{2+}\right)'$ by Zn^{2+} doping. This is because $\left(Zn_{Fe^{3+}}^{2+}\right)'$ can inhibit the $Fe^{3+} \rightarrow Fe^{2+}$ transition and also reduce the movement of oxygen vacancies by combining with $(V_{O^{2-}})^{\cdot\cdot}$ to form $\left[\left(Zn_{Fe^{3+}}^{2+}\right)' - (V_{O^{2-}})^{\cdot\cdot}\right]$ defect complexes. This

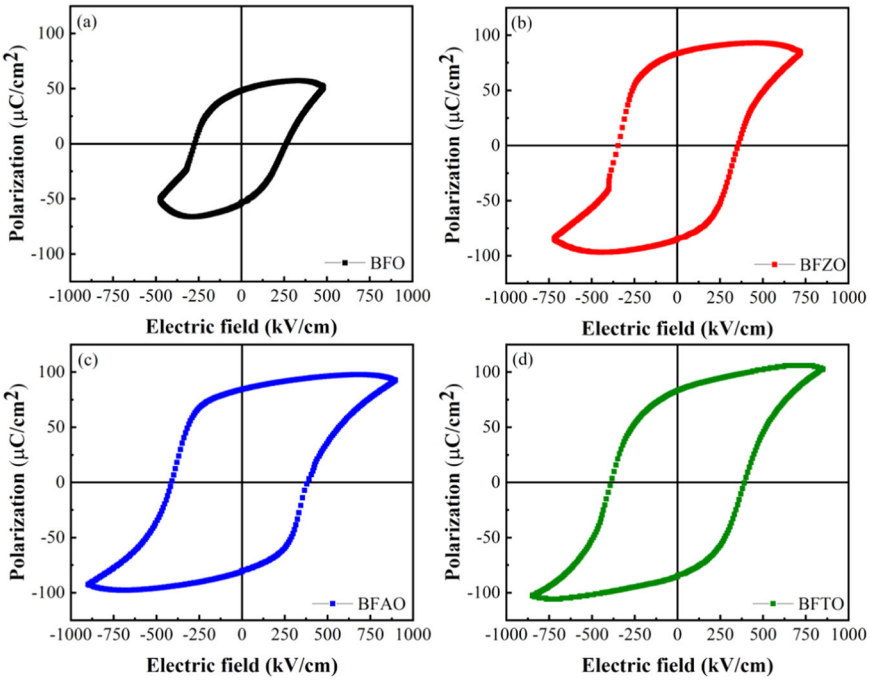

Fig. 6 Polarization–electric field hysteresis loops diagram (*P*–*E*) for pure BFO and $BiFe_{0.98}M_{0.02}O_3$ (M = Zn, Al, Ti) films

leads to drastic reduction of the leakage current and marked improvement of ferroelectric properties. The improvement of the ferroelectric properties of BFAO may be attributed to partial replacement of Fe^{3+} by Al^{3+}. Reduction in the proportion of Fe^{3+} may lead to a corresponding reduction in content of Fe^{2+}, which conversely reduces the $(V_{O^{2-}})^{\cdot\cdot}$ content to a certain extent. As a result, the leakage current of the films is reduced and the ferroelectric properties of BFO films are improved. Doped Ti^{4+} ions may combine with Fe^{2+} to form $Ti_{Fe}^{\cdot\cdot}$, or with Fe^{3+} to form Ti_{Fe}, which will suppress the generation of $(V_{O^{2-}})^{\cdot\cdot}$. The significant reduction in charge defects will greatly reduce leakage current, consequently improving ferroelectric properties of BFTO film [29]. In addition, a "lower head" phenomenon appears in the P-E diagram under a high electric field, which is caused by the existence of leakage current.

In order to further characterize the inherent ferroelectric properties of these films, meanwhile excluding the contribution of leakage current and nonlinear dielectric property to the polarization value of BFO films, positive-up-negative-down pulsed polarization tests were conducted for all four BFO films under a variable electric field with a fixed pulse width of 2.5 ms (i.e., $f \sim 1$ kHz). As shown in Fig. 7, the intrinsic polarization (ΔP) values of pure BFO, BFZO, BFAO and BFTO film samples are 85.45 μC/cm^2, 153.68 μC/cm^2, 149.47 μC/cm^2, and 150.10 μC/cm^2, respectively, at their corresponding maximum anti-breakdown electric fields. It can be seen that the (ΔP) values of BFZO, BFAO and BFTO films are close to the actual measured polarization values ($2P_r$), except for pure BFO films. This result indicates that (Zn^{2+}, Al^{3+}, Ti^{4+}) mono-doping can reduce the effect of nonlinear dielectric property and leakage current on the ferroelectric properties.

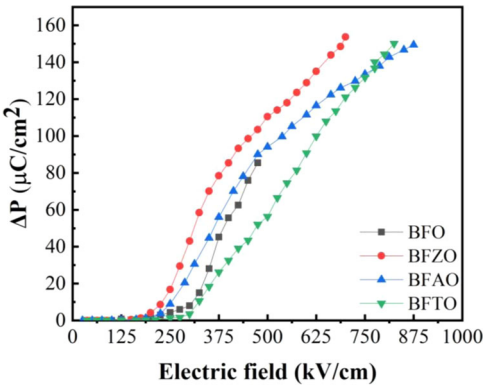

Fig. 7 PUND curves of pure BFO and $BiFe_{0.98}M_{0.02}O_3$ (M = Zn, Al, Ti) films

3.4 Dielectric constant and dielectric losses

As shown in Fig. 8, it can been seen the dielectric properties of BFO, BFZO, BFAO, and BFTO films in the application frequency range of 1 kHz–10 MHz. At application frequency of 10 kHz, the measured dielectric constant (ε_r) values for BFO, BFZO, BFAO, and BFTO films are 29.1, 35.3, 38.2, and 34.6, respectively. Moreover, the dielectric losses (tanδ) for BFO, BFZO, BFAO, and BFTO films are 0.12, 0.07, 0.02, and 0.03, respectively. It can be seen that BFZO, BFAO, and BFTO films have higher dielectric constant meanwhile the dielectric loss is lower than pure

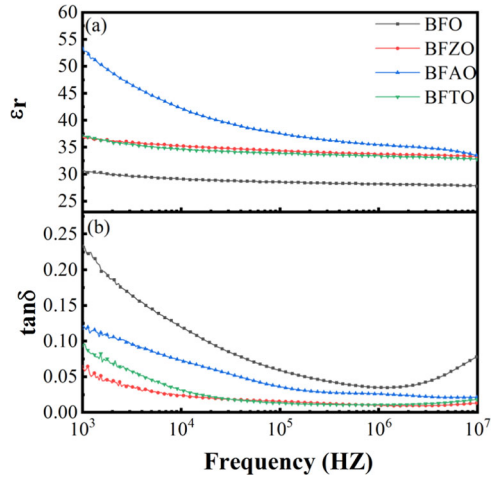

Fig. 8 Dielectric properties of pure BFO and $BiFe_{0.98}M_{0.02}O_3$ (M = Zn, Al, Ti) films, **a** dielectric constant ε_r **b** dielectric loss tanδ

BFO films, implying that (Zn^{2+}, Al^{3+}, Ti^{4+}) mono-doping improves the dielectric properties of BFO. And these properties of BFO are highly correlated with its microstructure and its ferroelectric polarization values [30, 31]. The improvement of ε_r and lower tanδ of (Zn^{2+}, Al^{3+}, Ti^{4+}) mono-doped BFO films may be related to their higher densities and significantly reduced irregular pinholes. In addition, the significantly improved dielectric properties of BFZO, BFAO, and BFTO films correspond to their increased remnant polarization values.

4 Conclusions

Spin-coated film samples of pure BFO and (Zn^{2+}, Al^{3+}, T^{i4+}) mono-doped $BiFe_{0.98}M_{0.02}O_3$ (M = Zn, Al, Ti) were favorably fabricated on FTO/glass substrates through sol–gel method. The results show that BFO film samples mono-doped with Zn^{2+}, Al^{3+}, and Ti^{4+} have rhombic distorted perovskite structure with R3m space group and no heterophases. Furthermore, the doping of these three elements with different valence states reduces the leakage current density of BFO films, significantly improves the ferroelectric remnant polarization, and improves the dielectric properties. Compared to pure BFO films, the leakage current density of $BiFe_{0.98}M_{0.02}O_3$ (M = Zn, Al, Ti) films is reduced by about three orders of magnitude, reaching 10^{-5} A/cm^2 under the applied electric field of 150 kV/cm. The $2P_r$ values of BFZO, BFAO, and BFTO film samples are 164.75, 168.66, and 168.24 μC/cm^2 at room temperature, respectively, which are much higher than that of pure BFO (102.36 μC/cm^2). This is mainly ascribed to the increased densities and significantly lower leakage current densities of the doped films. BFZO, BFAO, and BFTO films all have higher dielectric constants and reduced dielectric losses compared to pure BFO films, that may be caused to the improved densification and enhanced polarization of the films by (Zn^{2+}, Al^{3+}, Ti^{4+}) mono-doping. Our results provide valuable reference significance for the doping modification study of BFO films with different valence metal ions at Fe sites.

Acknowledgements This work is supported by the National Natural Science Foundation of China (Grant Nos. 52073129 and 51762030).

References

1. Catalan G, Scott JF (2009) Physics and applications of bismuth ferrite. Adv Mater 21:2463–2485
2. Wang JN, Li WL, Li XL, Fei WD (2013) Decreased crystallization temperature and improved leakage properties of $BiFeO_3$ thin films induced by Bi_2O_3 seed layer. Curr Appl Phys 13:2070–2075
3. Yun KY, Ricinschi D, Kanashima T, Noda M, Okuyama M (2004) Giant ferroelectric polarization beyond 150 μC/cm^2 in $BiFeO_3$ thin film. Jpn J Appl Phys 43:L647–L648
4. Hatt AJ, Spaldin NA, Ederer C (2010) Strain-induced isosymmetric phase transition in $BiFeO_3$. Phys Rev B 81:054109
5. Wang JL, Neaton JB, Zhang H, Nagarajan V, Ogale SB, Liu B, Viehland D, Vaithyanathan V, Schlom DG, Waghmare UV, Spaldin NA, Rabe KM, Wuttig M, Ramesh R (2003) Epitaxial $BiFeO_3$ multiferroic thin film heterostructures. Science 299: 1719–1722
6. Yoshimura T, Murakami S, Wakaono K, Kariya K, Fujimura N (2013) Piezoelectric vibrational energy harvester using lead-free ferroelectric $BiFeO_3$ films. Appl Phys Express 6:51501
7. She S, Yu J, Tang W, Zhu Y, Chen Y, Sunarso J, Zhou W, Shao Z (2018) Systematic study of oxygen evolution activity and arability on $La_{1-x}Sr_xFeO_{3-\delta}$ perovskite electrocatalysts in alkaline media. ACS Appl Mater Interfaces 10:11715–11721
8. Ma Z, Liu H, Wang L, Zhang F, Zhu L, and Fan S, Phase transition and multiferroic properties of Zr-doped $BiFeO_3$ thin films, J Mater Chem C https://doi.org/10.1039/d0tc04593d.
9. Wu J, Fan Z, Xiao D, Zhu J, Wang J (2016) Multiferroic bismuth ferrite-based materials for multifunctional applications: ceramic bulks, thin films and nanostructures. Prog Mater Sci 84:335
10. Dai ZH, Akishige Y (2010) Electrical properties of multiferroic $BiFeO_3$ ceramics synthesized by spark plasma sintering. J Phys D Appl Phys 43:445403
11. Lin F, Yu Q, Deng L, Zhang Z, He X, Liu X, Shi W (2017) Effect of La/Cr co-doping on structural transformation, leakage, dielectric and magnetic properties of $BiFeO_3$ ceramics. J Mat Sci 52:7118–7129
12. Lin Z, Cai W, Jiang W, Fu C, Li C, Song Y (2013) Effect of annealing temperature on the microstructure, optical, ferroelectric and photovoltaic properties of $BiFeO_3$ thin films prepared by sol-gel method. Ceram Int 39:8729–8736
13. Jin L, Tang X, Song D, Wei R, Yang J, Dai J, Song W, Zhu X, Sun Y (2015) Annealing temperature effect on (111)-oriented $BiFeO_3$ thin films deposited on Pt/Ti/SiO_2/Si by chemical solution deposition. J Mater Chem C 3:10742–10747
14. Guo Q, Sun H, Liu X, Sui H, Zhang Y, Zhou D, Liu P, Ruan Y (2017) Effect of excess Bi content on electrical properties of $BiFe_{0.95}Cr_{0.05}O_3$ thin films. J Mater Sci-Mater Electron 2017:7673

15. Xie X, Yang S, Zhang F, Fan S, Che Q, Wang C, Guo X, Zhang L (2015) Effect of excess Bi on structure and electrical properties of $BiFeO_3$ thin films desposited on indium tin oxide substrate using sol-gel method. J Mater Sci—Mater Electron 015:3693
16. Chung CF, Lin JP, Wu JM (2006) Influence of Mn and Nb dopants on electric properties of chemical-solution-deposited $BiFeO_3$ films. Appl Phys Lett 88:242909
17. Yang S, Zhang F, Xie X, Guo X, Zhang, L (2017) Effect of transition metal (Cu, Zn, Mn) doped on leakage current and ferroelectric properties of $BiFeO_3$ thin films. J Mater Sci-Mater El 8:7366
18. Liu H, Liu Z, Yao K (2007) Improved electric properties in $BiFeO_3$ films by the doping of Ti. J Sol-Gel Sci Technol 41:123–128
19. Zhang D, Shi P, Wu X, Ren W (2013) Structural and electrical properties of sol-gel- derived Al-doped bismuth ferrite thin films. Ceram Int 39:S461–S464
20. Sharma GN, Dutta S, Pandey A, Singh SK, Chatterjee R (2017) Microstructure and improved electrical properties of Ti-substituted $BiFeO_3$ thin films. Mater Res Bull 95:223–228
21. Haumont R, Kreisel J, Bouvier P et al. (2006) Phonon anomalies and the ferroelectric phase transition in multiferroic $BiFeO_3$. Phys Rev B 73:132101
22. Liu WL, Tan GQ, Dong GH et al. (2014) Structure transition and multiferroic properties of Mn-doped $BiFeO_3$ thin films. J Mater Sci -Mater Electron 25:723–729
23. Benali A, Melo BMG, Prezas PR, Bejar M, Dhahri E, Valente MA, Graca MPF, Nogueira BA, Costa BFO (2019) Structural, morphological, Raman and ac electrical properties of the multiferroic sol-gel made $Bi_{0.8}Er_{0.1}Ba_{0.1}Fe_{0.96}Cr_{0.02}Co_{0.02}O_3$ material. J Alloy Compd 775:304–315
24. Dong G, Tan G, Luo Y, Liu W, Ren H, Xia A (2014) Structural transformation and multiferroic properties of single-phase $Bi_{0.89}Tb_{0.11}Fe_{1-x}Mn_xO_3$ thin films. Appl Surf Sci 290:280–286
25. Shuai Y, Zhou S, Burger D, Helm M, Schmidt H (2011) Nonvolatile bipolar resistive switching in Au/$BiFeO_3$/Pt. J Appl Phys 109:124117
26. Wang J, Luo L, Han C, Yun R, Tang X, Zhu Y, Nie Z, Zhao W, Feng Z (2019) The microstructure, electric, optical and photovoltaic properties of $BiFeO_3$ thin films prepared by low-temperature sol-gel method. Materials 12:1444
27. Hu Z, Li M, Yu Y, Liu J, Pei L, Wang J, Liu X, Yu B, Zhao X (2010) Effect of Nd and high-valence Mn co-doping on the electrical and magnetic properties of multiferroic $BiFeO_3$ ceramic. Solid State Commun 150:1088–1091
28. Wang Y, Nan C-W (2006) Enhanced ferroelectricity in Ti-doped multiferroic $BiFeO_3$ thin films. Appl Phys Lett 89:052903
29. Raghavan CM, Kim JW, Kim SS (2014) Effect of Ho and Ti doping on structural and electrical properties of $BiFeO_3$ thin films. J Am Ceram Soc 97:235–240
30. Yun KY, Noda M, Okuyama M, Saeki H, Tabata H, Saito K (2004) Structural and multiferroic properties of $BiFeO_3$ thin films at room temperature. J Appl Phys 96:3399–403
31. Das SR, Bhattacharya P, Choudhary RNP, Katiyar RS (2006) Effect of La substitution on structural and electrical properties of $BiFeO_3$ thin film. J Appl Phys 99:066107